arXiv:1512.03943v1 [physics.flu-dyn] 12 Dec 2015

Turbulent 2.5 dimensional dynamos

K. Seshasayanan[1]† and A. Alexakis[1]

[1]Laboratoire de Physique Statistique, École Normale Supérieure, CNRS UMR 8550, Université Paris Diderot, Université Pierre et Marie Curie, 24 rue Lhomond, 75005 Paris, France

(Received xx; revised xx; accepted xx)

We study the dynamo instability driven by a turbulent two dimensional flow with three components of the form $(u(x, y, t), v(x, y, t), w(x, y, t))$ sometimes referred to as a 2.5 dimensional flow. This type of flows provides an approximation to very fast rotating flows often observed in nature. The low dimensionality of the system allows the investigation of a wide range of fluid Reynolds number Re, magnetic Reynolds number Rm and forcing length scales relative to the domain size that is still prohibited for full three dimensional numerical simulations. We were thus able to determine the properties of the dynamo onset as a function of Re and and the asymptotic behavior of the most unstable mode in the large Rm limit. In particular it has been shown that: In a non-helical flow in an infinite domain the critical magnetic Reynolds number Rm_c becomes a constant in the large Re limit. A helical flow always results in dynamo in agreement with mean field predictions. For thin layers for both helical and nonhelical flows the Rm_c scales as a power-law of Re. The growth-rate of fastest growing mode becomes independent of Re and Rm when their values are sufficiently large. The most unstable length scale in this limit scales linearly with the forcing length scale. Thus while the mean field predictions are valid, they are not expected to be dominant in the large Rm limit.

Key words:

1. Introduction

The dynamo instability caused by the motion of conducting fluids is used to explain the existence of magnetic fields in astrophysical objects. In many cases these objects are rotating rendering the resulting flow strongly anisotropic (Pedlosky 1987; Izakov 2013). In rotating flows the Coriolis force suppresses the fluctuations along the axis of rotation as shown by the the Taylor-Proudmann theorem. Thus very fast rotating flows become to some extent two-dimensionalized depending only on two spacial coordinates while retaining in some cases all three velocity components depending on the boundary conditions. The two-dimensionalization of such flows have been shown in theoretical investigations (Waleffe 1993; Hopfinger & van Heijst 1993; Scott 2014), numerical simulations (Hossain 1994; Yeung & Zhou 1998; Smith & Waleffe 1999; Chen *et al.* 2005; Thiele & Müller 2009; Mininni & Pouquet 2010; Yoshimatsu *et al.* 2011; Sen *et al.* 2012; Deusebio *et al.* 2014; Alexakis 2015) and laboratory experiments (Sugihara *et al.* 2005; Staplehurst *et al.* 2008; van Bokhoven *et al.* 2009; Yarom *et al.* 2013; Campagne *et al.* 2014; Gallet *et al.* 2014). Recently a theoretical work showed that the flow becomes exactly two-dimensional provided that the rotation is above a critical value (Gallet 2015).

† Email address for correspondence: skannabiran@lps.ens.fr

This allows one to consider the limit of infinite rotation which leads to a flow of the form $(u(x,y,t), v(x,y,t), w(x,y,t))$. This flow is independent of the coordinate along the axis of rotation (from here on taken as the z-direction). These flows are referred in literature as $2.5D$ flows or $2+\epsilon$ model.

Rotation is known to play an important role in dynamo instability (Proctor & Gilbert 1995; Davidson 2014). A $2.5D$ flow is one of the simplest flow configuration that can result to dynamo since a two-dimensional two-component flow does not give rise to dynamo instability (Zel'dovich 1958). Thus, various studies have been performed in different limits. One of the first studies was by Roberts (1972) that considered the dynamo instability of four different laminar time independent 2.5D flows. Time dependent but laminar 2.5D flows allow for the presence of chaos and thus pose a computationally tractable system to investigate the existence of the fast dynamos (dynamos whose growth rate remains finite in the high conductivity limit) that was investigated in Galloway & Proctor (1992), as well as the behaviour of large scale dynamo action (alpha dynamos) in the same limit (see Courvoisier *et al.* (2006)). Studies of turbulent 2.5D flows were first studied to our knowledge by Smith & Tobias (2004), where a helical forcing was considered. In their configuration the inverse cascade of energy led to a large scale condensate which drove the dynamo instability. The role of these large scale coherent structures were further studied in (Tobias & Cattaneo 2008) where a differentiation between the scales responsible for the dynamo was made using spectral filters.

The present work focuses on turbulent 2.5D dynamos in the absence of large scales condensates. Condensates form when an inverse cascade is present and there is no large scale dissipation mechanism to saturate the energy growth. Such a large scale dissipation mechanism is often provided by Ekman Friction (Pedlosky 1987) that leads to a linear damping. In its absence energy piles in the largest scales of the domain until it is balanced by viscosity. This leads to the formation of very large amplitude vortices. However the turn-over time of the condensate vortices becomes comparable to the rotation period and the condition for quasi-two-dimensionalization is violated, with the flow becoming three dimensional again (Bartello *et al.* 1994; Alexakis 2015). For this reason we only consider here turbulent 2.5D flows in the presence of linear damping that limits the cascade to scales smaller than the domain size.

The study is based on numerical simulations of 2.5D turbulence in a two dimensional periodic box. Helical and non-helical flows are both considered. The focus is on covering a wide range of parameter space for both types of forcing. We describe the system in detail in Section 2 and discuss the hydrodynamic cascades that happen in this set-up in Section 3. The results for the helical forcing are presented in Section 4 and for the non-helical forcing in Section 5. The critical magnetic Reynolds number is discussed in section 6. The dependence of the dynamo instability with respect to the forcing length-scale is discussed in Section 7. We present our conclusions in Section 8.

2. Governing equation

We consider a $2.5D$ flow in a box of size $[2\pi L, 2\pi L, H]$ with the height H being along the invariant direction z. The equations governing the velocity field $\mathbf{u} = \mathbf{u}_{2D} + u_z\hat{\mathbf{e}}_z = \nabla\times(\psi\hat{\mathbf{e}}_z) + u_z\hat{\mathbf{e}}_z$ are,

$$\begin{aligned} \partial_t \Delta\psi + (\nabla\times\psi\hat{\mathbf{e}}_z)\cdot\nabla\,\Delta\psi &= \nu\,\Delta^2\psi - \nu_{_h}\,\Delta\psi + \Delta f_\psi \\ \partial_t u_z + (\nabla\times\psi\hat{\mathbf{e}}_z)\cdot\nabla u_z &= \nu\,\Delta u_z + f_z \end{aligned} \tag{2.1}$$

where ν is the small scale dissipation coefficient, $\nu_{_h}$ is the large scale dissipation coefficient. The vertical velocity u_z is advected as a passive scalar. We force the velocity

TABLE 1. Range of values of each parameter explored in the DNS. N is the numerical resolution in each direction and T is the typical eddy turn over time over which the growth rate is calculated.

Case	A1	A2	A3
$k_f L$	4	8	16
N	$[256, 2048]$	$[512, 2048]$	$[512, 2048]$
Re	$[0.5, 1200]$	$81, 92$	$91, 97$
Rm	$[0.1, 2000]$	$[0.5, 1000]$	$[0.5, 1000]$
T	$[300, 2000]$	$[300, 600]$	$[300, 600]$

fields with the forcing: f_ψ, f_z. Two forcing functions are used to study this problem, one with mean helicity and the other without any mean helicity. More precisely the forcing functions are, $f_\psi = f_z = \cos(k_f x) + \sin(k_f y)$ for the helical case and $f_\psi = \cos(k_f x) + \sin(k_f y)$, $f_z = \sin(k_f y) + \cos(k_f x)$ for the nonhelical case. It is easy to note that for the helical case the helicity of the forcing given by $\langle f_z \Delta f_\psi \rangle \neq 0$ whereas for the nonhelical case it is zero.

Due to the invariance in the z direction the magnetic field can be decomposed into Fourier modes in z, $\mathbf{B} = \mathbf{b}(x, y, t)\, exp(ik_z z)$. Each mode evolves independently and is governed by the induction equation,

$$\partial_t \mathbf{b} + (\nabla \times \psi \hat{\mathbf{e}}_z) \cdot \nabla \mathbf{b} + u_z i k_z \mathbf{b} = \mathbf{b} \cdot \nabla\ (\nabla \times \psi \hat{e}_z) + \eta\ \left(\Delta - k_z^2\right) \mathbf{b} \tag{2.2}$$

where η is the magnetic diffusion. The divergence free condition $\nabla \cdot \mathbf{B} = 0$ for each magnetic mode gives,

$$\partial_x b_x(x, y, t) + \partial_y b_y(x, y, t) = -i k_z b_z(x, y, t). \tag{2.3}$$

The non-dimensional control parameters of this system are the $Re = \left\langle |\mathbf{u}|^2 \right\rangle^{1/2} L/\nu$ the fluid Reynolds number, $Rm = \left\langle |\mathbf{u}|^2 \right\rangle^{1/2} L/\eta$ the magnetic Reynolds number, $k_f L$ the forcing wavenumber. Given the set of non-dimensional parameters we look for the range of modes $k_z L$ that become unstable.

The equations are solved numerically on a double periodic domain of size $[2\pi L, 2\pi L]$ using a standard pseudo-spectral scheme and a Runge-Kutta fourth order scheme for time integration (see Gomez *et al.* (2005)). The initial condition for both the magnetic and the kinetic field is sum of a few Fourier modes with random phases. Initially a hydrodynamic steady state is obtained by solving only the hydrodynamic equations at a particular $Re, k_f L$. With this steady state the dynamo simulation is begun with a seed magnetic field and evolving both the velocity and the magnetic field. The magnetic field starts to grow or decay depending on the control parameters in the system. We define the growth rate of the magnetic field as,

$$\gamma = \lim_{t \to \infty} \frac{1}{2t} log \frac{\left\langle |\mathbf{b}|^2(t) \right\rangle}{\left\langle |\mathbf{b}|^2(0) \right\rangle} \tag{2.4}$$

as a function of the non-dimensional parameters $Re, Rm, k_z L, k_f L$. A table of runs is shown in table 1 indicating the range of values of each parameters examined.

3. Hydrodynamic cascades

We first describe the hydrodynamic structure of the flow. The quantities conserved by the nonlinearities in the hydrodynamic equations are, the enstrophy in $x - y$ plane

$\Omega = \langle \omega_z^2 \rangle$ with $\omega_z = -\Delta\psi$ and the angular brackets $\langle\cdot\rangle$ denote spatial average, the energy in $x-y$ plane, $E_{_{2D}} = \langle \mathbf{u}_{_{2D}} \cdot \mathbf{u}_{_{2D}} \rangle /2$, the energy of the z component of velocity $E_{_Z} = \langle u_z^2 \rangle /2$ and the helicity $H = \langle u_z\, \omega_z \rangle$. For a more detailed discussion on the invariants see Smith & Tobias (2004). For sufficiently small viscosity ν and damping ν_h the conserved quantities cascade either to the small or the large scales. For the $2D$ flow we have a forward cascade of enstrophy Ω and an inverse cascade of energy $E_{_{2D}}$. The E_z has a forward cascade since u_z is advected like a passive scalar. We mention that even when the forcing is with maximum helicity $f_z \propto f_\psi$ the governing equation for u_z is not the same as the vorticity ω_z due to the presence of large scalar damping. Helicity cascades to small scales since both E_z, Ω cascade to small scales. Between the forcing scale and the dissipation scale there exists a range of scales (the inertial range) where the energy spectra have a power law behaviour. The exponents of these power laws are determined by the cascading quantities in the classical Kolmogorov approach. The exponents in this setup, for $E_{_{2D}}$, is -3 in the scales smaller than the forcing scale due to enstrophy cascade and $-5/3$ in the scales larger than the forcing scale due to the inverse energy cascade. Similarly for the spectra of E_z we have -1 in the scales smaller than the forcing scale due to the forward cascade of the passive scalar E_z like the spectra of the variance of a passive scalar (Batchelor 1959). Since there are no inverse cascade for u_z we expect an equipartition exponent of $+1$ at scales larger than the forcing scale.

Figure 1 shows the spectra $E_{_{2D}}$ and E_z for different values of Re for nonhelical forcing. The spectra of the helical forcing case are very similar to the spectra of the flows with nonhelical forcing so they are not shown here. The figure shows that the exponents of $E_{_{2D}}$ and E_z in the forward cascade change as we increase the Re. As shown in Boffetta (2007) the exponent for the energy spectra in the small scales tend to the expected value of -3 as the Re becomes large. In their study they went upto 32768^2 to get the expected k^{-3} spectrum. In this work since the focus is on the dynamo effect the simulations are done only upto 2048^2, thus the exponent in the spectra is less than -3. Figure 2 shows the spectra $E_{_{2D}}$ and E_z as $k_f\, L$ is varied for the nonhelical forcing. Due to the presence of an inverse cascade the energy spectra form a $k^{-5/3}$ for scales larger than the forcing scale. While for the vertical velocity spectra the large scales form an equipartition spectrum of k^{+1}. The inverse cascade of energy is dissipated by the friction at large scales which inhibits the formation of a large scale condensate.

The transfer of energy to the magnetic field from the kinetic field in the dynamo problem is related to the shear of the velocity field. In $2D$ turbulence, the shear $S^\ell_{_{2D}}$ in $\mathbf{u}_{_{2D}}$ at a scale ℓ can be estimated by $S^\ell_{_{2D}} \propto u^\ell_{_{2D}}/\ell$ where $u^\ell_{_{2D}}$ is the amplitude of the $\mathbf{u}_{_{2D}}$ at a scale ℓ. For $2D$ turbulence $S^\ell_{_{2D}}$ is same at all scales between the forcing and the small scale dissipation since $u^\ell_{_{2D}} \sim \ell$. Thus for any $\ell_f > \ell > \ell_\nu$ we have $S^\ell_{_{2D}} \ell_f / u_f \sim \mathcal{O}(1)$. This is strictly true for a spectra of k^{-3}, which is seen at very large Re. Since most of the study presented here is with an exponent less than -3 the shear $S_{_{2D}}$ is dominated at the forcing scale k_f. For the vertical velocity field the shear can be estimated by $S^\ell_z \propto u^\ell_z/\ell$, where u^ℓ_z is the magnitude of u_z at scale ℓ. It is dominated at the smallest scales and we have $S^{\ell_\nu}_z \ell_f / u_f \sim Re^{1/2}$. Thus shear is dominated at forcing scale for $\mathbf{u}_{_{2D}}$ while for u_z it is dominated at the viscous scales. However the dynamo instability requires the presence of both S_z and S_ℓ. Thus we can not a priori determine which scales will be responsible for dynamo action. We remark that the dominant shear scales present here differ from the condensate regime where all the shear is dominated at the scale of the box.

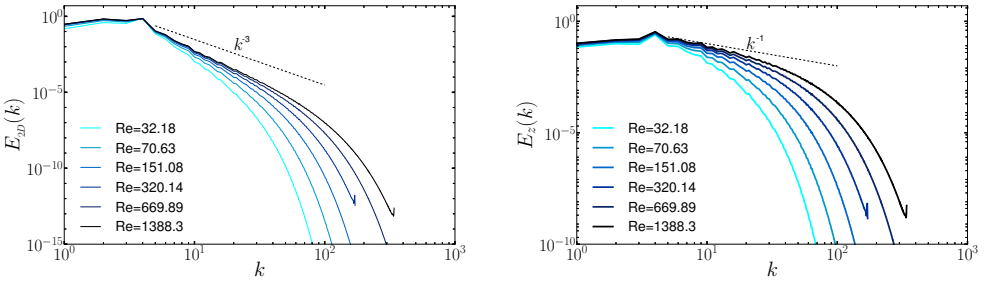

FIGURE 1. Plot shows the spectra of the $2D$ kinetic energy $E_{_{2D}}(k)$ and the spectra of the vertical velocity $E_z(k)$ for different values of Re mentioned in the legend. The spectra correspond to nonhelical forcing case.

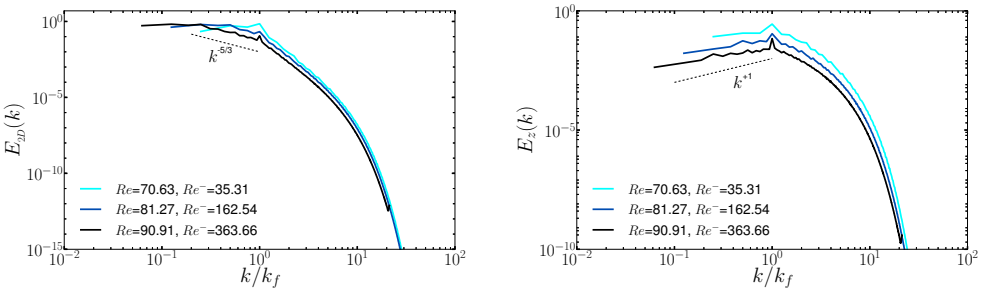

FIGURE 2. Plot shows the spectra of the $2D$ kinetic energy $E_{_{2D}}(k)$ and the spectra of the vertical velocity E_z as a function of the rescaled wavenumber k/k_f for different values of Re and $k_f\,L$ mentioned in the legend. The spectra correspond to the nonhelical forcing case.

4. Helical forcing

4.1. *Dependence of γ on k_z*

We first focus on the helical forcing, the laminar case of which corresponds to the case studied by Roberts (1972). Figure 3 shows the growth rate γ as a function of k_z for different values of Rm that are mentioned in the legend and for a fixed $Re \approx 46$. The number of unstable k_z modes increases as we increase Rm as has been observed in other laminar and turbulent studies Roberts (1972); Tobias & Cattaneo (2008); Smith & Tobias (2004). As we increase Rm the growth rates for small $k_z \sim \mathcal{O}(1)$ saturates.

There are dynamo unstable modes for all values of Rm, but the range of unstable modes become smaller as Rm is reduced. This can be attributed to the α-effect which is a mean field effect that can amplify the magnetic field at arbitrarily large scales. In the mean field description the large scale magnetic field $\overline{\mathbf{B}}$ obeys the equation

$$\partial_t \overline{\mathbf{B}} = \nabla \times (\alpha \overline{\mathbf{B}}) + \eta_{\mathbf{T}} \Delta \overline{\mathbf{B}} \tag{4.1}$$

where α is in general a tensor and η_T is the turbulent diffusivity. For isotropic flows the diagonal terms in the α tensor are equal and are responsible for the dynamo effect. They can be calculated numerically by imposing a uniform magnetic field $\mathbf{B}_0$ and measuring the induced field $\mathbf{b}$, (see Courvoisier *et al.* (2006)).

$$\alpha \cdot \mathbf{B}_0 = \langle \mathbf{u} \times \mathbf{b} \rangle \tag{4.2}$$

$$\partial_t \mathbf{b} + \mathbf{u} \cdot \nabla \mathbf{b} = \mathbf{b} \cdot \nabla \mathbf{u} + \mathbf{B}_0 \cdot \nabla \mathbf{u} + \eta \Delta \mathbf{b} \tag{4.3}$$

In the small Rm limit, $\eta_T = \eta$ and the α coefficient can be calculated analytically (see

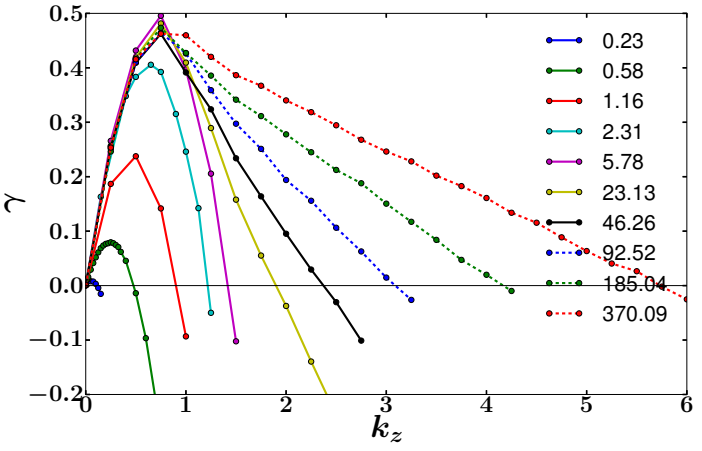

FIGURE 3. Plot shows the growth rate γ as a function of k_z for the helical forcing case for different values of Rm mentioned in the legend for a $Re \approx 46$.

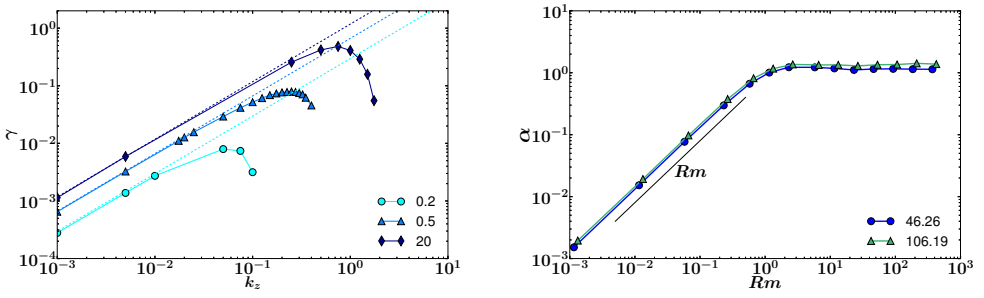

FIGURE 4. The figure on the left shows the growth rate γ as a function of k_z in log-log scale. The corresponding α values are shown by the dotted straight lines at values of Rm mentioned in the legend. The figure on the right shows α as a function of Rm for two different Re mentioned in the legend.

Childress (1969); Gilbert (2003)) leading to the scaling $\alpha \sim u\,Rm$. In either case the resulting growth rate for the problem at hand is given by

$$\gamma = \alpha\, k_z - \eta_T\, k_z^2. \tag{4.4}$$

The left panel of figure 4, shows the $\gamma - k_z$ curve in log-log scale with the straight lines indicating the linear scaling $\alpha\, k_z$ with α calculated from equations 4.2, 4.3. This demonstrates that the behaviour of γ in the small k_z limit is described well by the α-effect. The right panel of figure 4 shows the dependence of α as a function of Rm for two different Re. For a turbulent flow and for small Rm we expect the α coefficient to scale like $\alpha \sim u\,Rm$, see Gilbert (2003), which is captured well by the numerical data. For large Rm the α value saturates to a constant of the same order as the velocity field. This is different from what has been observed in chaotic flows in Courvoisier *et al.* (2006), where the α coefficient varies rapidly as one increases Rm.

Figure 5 shows the total magnetic energy spectra $E_B(k)$ for different values of Rm and a fixed $k_z = 0.25$ and $Re \approx 530$. When the α effect is more pronounced, the magnetic spectra is concentrated at large scales. This occurs in the small Rm limit. For large Rm the magnetic energy spectra becomes more concentrated towards smaller scales.

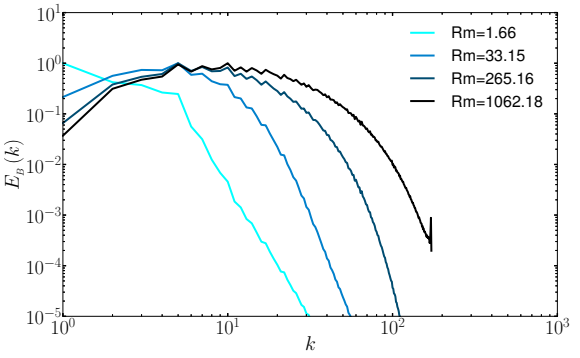

FIGURE 5. Plot shows the magnetic energy spectra $E_B(k)$ as a function of the wavenumber k for different Rm shown in the legend. These correspond to a Reynolds number $Re \approx 530$ and to the helical forcing case.

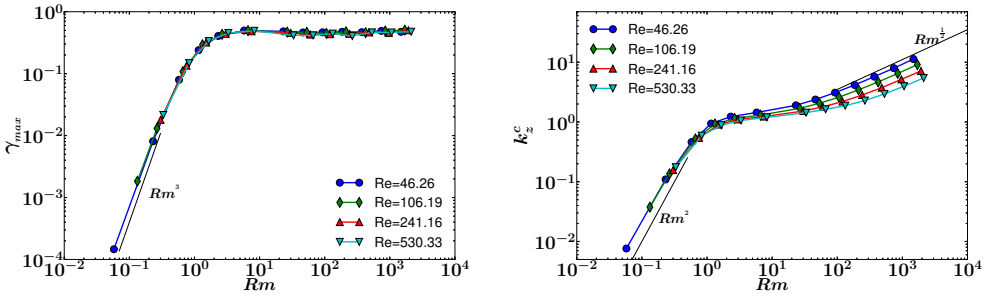

FIGURE 6. Figure shows γ_{max} on the left and k_z^c on the right as a function of Rm for different values of Re mentioned in the legend for the helical forcing case.

4.2. γ_{max} *and* k_z^c

To quantify the behaviour of γ as we change both Re and Rm we define two quantities γ_{max} and k_z^c which characterize the curves shown in figure 3. γ_{max} is the maximum growth rate for a given Re, Rm whereas k_z^c is the largest k_z that is dynamo unstable for a given Re, Rm. Figure 6 shows γ_{max} and k_z^c as functions of Rm for different values of Re. It can be seen that γ_{max} is independent of Re and becomes saturated for $Rm \sim \mathcal{O}(1)$. In the small Rm limit the behaviour of γ_{max} is governed by the α-effect, which gives a scaling $\gamma_{max} \propto Rm^3$ obtained by finding the maximum of equation 4.1. For large Rm the γ_{max} remains a constant thus it is a fast dynamo. The most unstable length scale is in between the forcing scale and scale of the box and not in the small k_z region.

In the plot of k_z^c in the small Rm limit the behaviour is dominated by the α-effect where $k_z^c \propto Rm^2$ obtained from equation 4.1. In this limit the behaviour of k_z^c does not depend on Re since $k_z^c = cRm^2$ with c being independent of Re. For large values of Rm we see the scaling $k_z^c \propto Rm^{1/2}$ which can be obtained by balancing the ohmic dissipation with the stretching term. We can also see a clear decrease with the increase of Re which will be discussed in section 6.1.

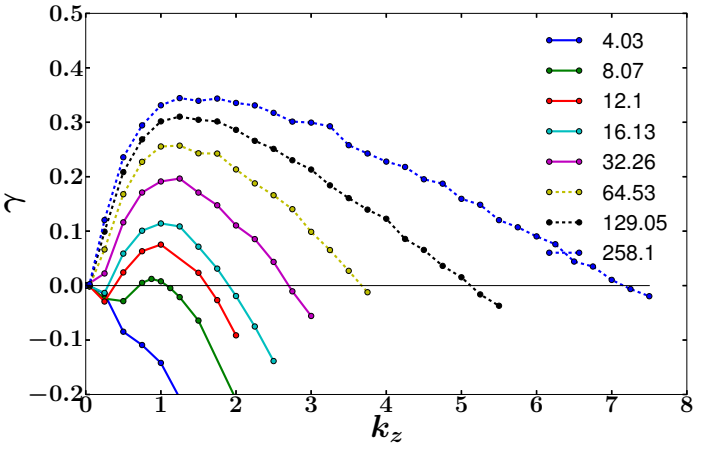

FIGURE 7. Plot shows the growth rate γ as a function of k_z for different values of Rm mentioned in the legend for a $Re \approx 32$. The curves correspond to the nonhelical forcing case.

5. Nonhelical forcing

5.1. *Dependence of γ on k_z*

The growth rate γ is shown as a function of k_z for different values of Rm in figure 7. Unlike the helical case, there is no dynamo for small Rm due to the absence of a mean-field α-effect. For sufficiently large Rm dynamo instability occurs with the magnetic spectra concentrated in the small scales similar to the large Rm case of the helical forcing shown in figure 5. As Rm is increased the number of unstable modes increase as the ohmic dissipation becomes smaller.

5.2. *γ_{max} and k_z^c*

Figure 8 shows γ_{max} and k_z^c as a function of Re, Rm. The dynamo instability starts at a $Rm \approx 10$ which is the critical magnetic Reynolds number for this type of forcing. Unlike the helical case the maximum growth rate γ_{max} increases slowly with Rm and a clear asymptote has not yet been reached. Re does not seem to affect the behaviour of the γ_{max} curve indicating that the most unstable modes are not affected by the smallest viscous scales. The scaling of $k_z^c \sim Rm^{1/2}$ in the large Rm limit is observed with a prefactor that decreases as Re is increased similar to the helical case. The magnetic field generated in the small scales is spatially concentrated in thin filamentary structures. Figure 9 shows the contours of magnetic energy in the plane - $|B_{2D}|^2 = |b_x|^2 + |b_y|^2$ for increasing values of the magnetic Reynolds number Rm. These structures become thiner as we increase Rm with the thickness scaling like $Rm^{-1/2}$. This gives a physical interpretation for the scaling $k_z^c \sim Rm^{1/2}$ seen in figures 6, 8 in terms of H: these filaments should be thinner than the box height H for the dynamo instability to take place.

6. Critical magnetic Reynolds number Rm_c

6.1. *Finite layer thickness*

In general the onset of the dynamo instability depends on the domain size since it determines the available wavemodes. For a given height H the allowed wavenumbers satisfy $k_z \geqslant 2\pi/H \equiv k_z^H$. We thus define a critical magnetic Reynolds number Rm_c

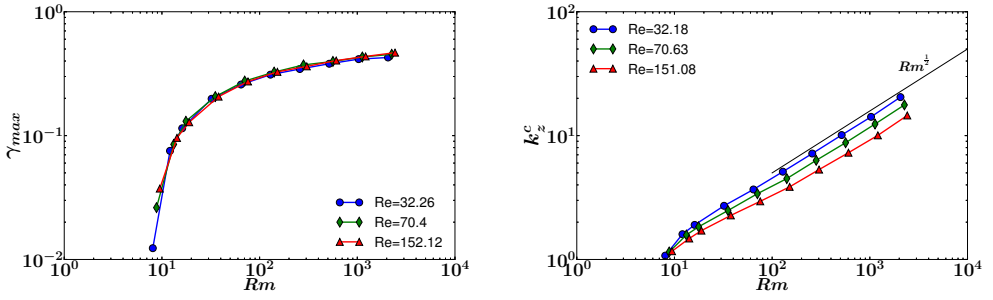

FIGURE 8. Figures shows γ_{max} on the left and k_z^c on the right as a function of Rm for different values of Re mentioned in the legend. The curves correspond to the nonhelical forcing case.

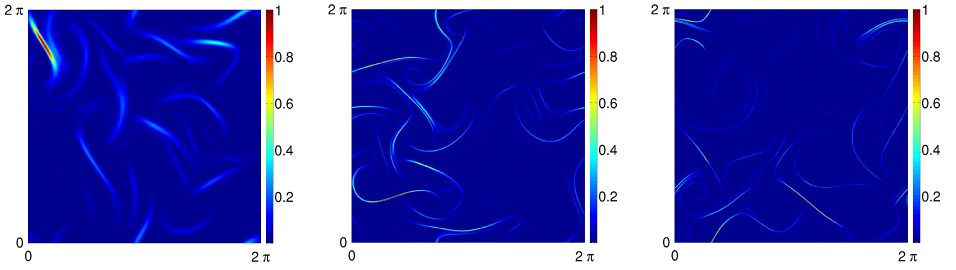

FIGURE 9. Contour of the magnetic energy $B_{_{2D}}$ for different values of Rm, from left to right we have, $Rm \approx 32$, $Rm \approx 1030$, $Rm \approx 2060$ with the $Re \approx 32$ for all the three contours. The figures correspond to the nonhelical forcing case.

based on H as,

$$Rm_c^H\ \left(Re, k_z^H\right)\ =\ \max\left\{Rm\ \text{ s.t. }\ \gamma \leqslant 0\quad \forall k_z > k_z^H\right\}. \tag{6.1}$$

The dynamo instability then only exists for $Rm > Rm_c^H$. The value Rm_c^H can be calculated from the figures 6,8 imposing that the marginal k_z for dynamo equals the minimum allowed wavenumber $k_z^c(Re, Rm) = k_z^H$. For the helical case in the small Rm limit we get the relation $Rm_c^H \propto \sqrt{k_z^H}$ based on the α-effect. Thus for large H a small Rm is sufficient for dynamo instability $Rm_c^H \propto (H)^{-1/2}$ with the proportionality coefficient being independent of Re.

The behaviour of Rm_c^H for thin layers ($k_z^H \gg k_f$) depends on Re for both the forcing cases considered. In order mesure this dependence on Re, we rescale k_z^c with Re and replot it as a function of Rm. Figure 10 shows the rescaled cut-off wavenumber $k_z^c\, Re^{\zeta}$ for the two different types of forcing studied. Here ζ is an exponent used to collapse the data at large k_z. For the helical forcing we find a best fit of $\zeta = 0.37\cdots \approx 3/8$ and for the nonhelical forcing we find a best fit of $\zeta = 0.25\cdots \approx 1/4$. This implies that the critical magnetic Reynolds number scales like $Rm_c^H \propto Re^{2\zeta}\sqrt{k_z^H}$. This is unlike the three dimensional dynamos where Rm_c is found to reach a constant value in the large Re limit. However, given that $\zeta < 1/2$, in the limit of large Re, $Rm_c^H \ll Re$ thus like three dimensional turbulence dynamo can be achieved for any Prandtl number $Pm = Rm/Re$ provided R_m is large enough. Whether this behaviour persists for very large Re remains to be seen.

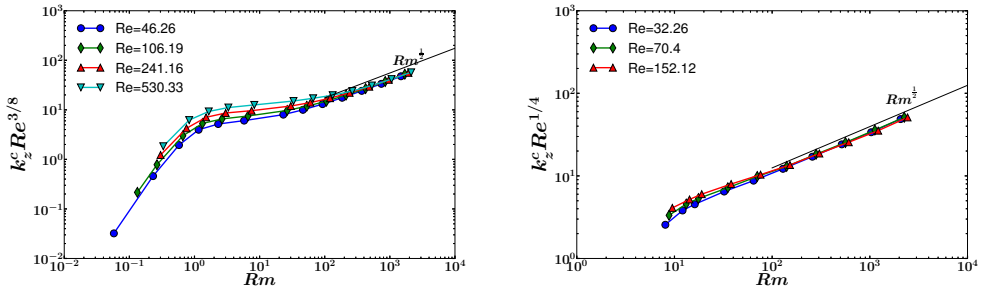

FIGURE 10. Figure shows $k_z^c\, Re^{\zeta}$ as a function of Rm for different values of Re shown in the legend, for the helical forcing case shown on left and the nonhelical forcing case shown on the right.

6.2. *Infinite layer thickness*

As seen in figure 3, in helical flows due to the α-effect for any Rm there always exists k_z small enough such that the modes are dynamo unstable. Thus for a layer that is infinitely thick, a helical flow does not have a critical magnetic Reynolds number since unstable modes exist even for $Rm \to 0$. For the nonhelical case however there is a critical Rm for the dynamo instability as can be seen in figures 7, 8. Below this Rm_c for any mode k_z there is no dynamo instability. Thus the critical magnetic Reynolds number Rm_c in the infinite domain is defined as,

$$Rm_c\ (Re)\ =\ \max\left\{Rm\ \text{ s.t. }\ \gamma \leqslant 0\quad \forall k_z\right\} = \lim_{H\to\infty} Rm_c^H. \tag{6.2}$$

Note that in practice we do not need an infinitely thick layer to capture the onset of the instability. The height H however needs to be sufficiently large so that it allows the first unstable mode $k_z \simeq 1$ (as can be seen in figure 7) to be present. The dependence of Rm_c as a function of Re can be seen in the figure 11. Three different regimes corresponding to different flow behaviours are identified and are separated by vertical dotted lines in the figure denoting the critical Reynolds numbers Re_{T_1}, Re_{T_2}. The curve for $Re > Re_{T_2}$ corresponds to the turbulent regime at large Re and the curves in $Re < Re_{T_1}$, $Re_{T_1} < Re < Re_{T_2}$ correspond to two different laminar flows. Here Re_{T_2} is the Reynolds number at which the flow transitions between a turbulent state and a laminar state. While Re_{T_1} is the Reynolds number at which the flow transitions between two different laminar time independent flows. In the limit of large Re we see that the value of Rm_c saturates as is observed in $3D$ turbulent flows Ponty *et al.* (2005); Iskakov *et al.* (2007); Mininni (2007). Across the transition Reynolds numbers Re_{T_2} and Re_{T_1}, the Rm_c curves have discontinuous behaviour because the flow transitions from one state to the other subcritically. In these laminar states we find that the growth rate γ scales as k_z^2 for very small k_z as shown in figure 12 for a $Re = 0.91 < Re_{T_1}$ in the laminar regime. This scaling indicates that the dynamo action can be explained by the β-effect, also known in literature as the negative magnetic diffusivity effect, (see Lanotte *et al.* (1999)). The β-effect is a mean-field effect and the magnetic field is amplified also at the large scales. Figure 13 shows the contour of the $|B_{2D}|^2 = |b_x|^2 + |b_y|^2$ which is the energy of the magnetic field in the $x-y$ plane. Two different Reynolds number are shown, on the left $Re_{T_1} < Re = 5.4 < Re_{T_2}$ and on the right $Re = 0.53 < Re_{T_1}$ corresponding to the two different laminar states. Both the plots show large scale modulations in the magnetic energy at scales close to the box size.

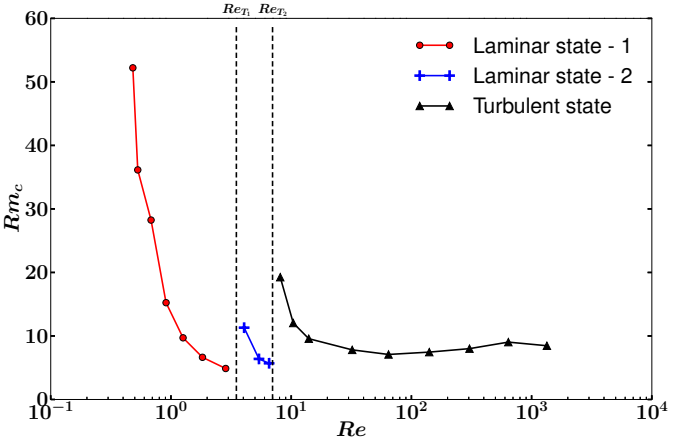

FIGURE 11. Plot shows the critical magnetic Reynolds number Rm_c as a function of the fluid Reynolds number Re. Two vertical dotted lines denote the two transition Reynolds numbers Re_{T_1}, Re_{T_2}. The curves correspond to the nonhelical forcing case.

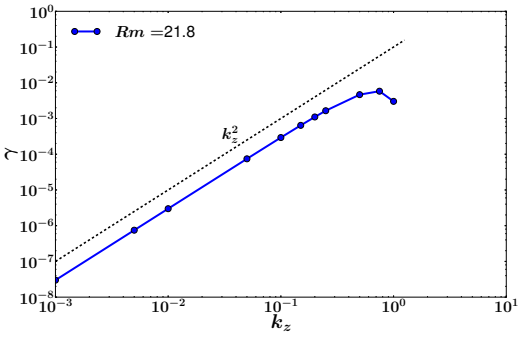

FIGURE 12. Plot shows the growth rate γ as a function of k_z for a Reynolds number $Re = 0.91 < Re_{T_1}$ is shown along with the dotted line with the scaling k_z^2. The curve correspond to the nonhelical forcing case.

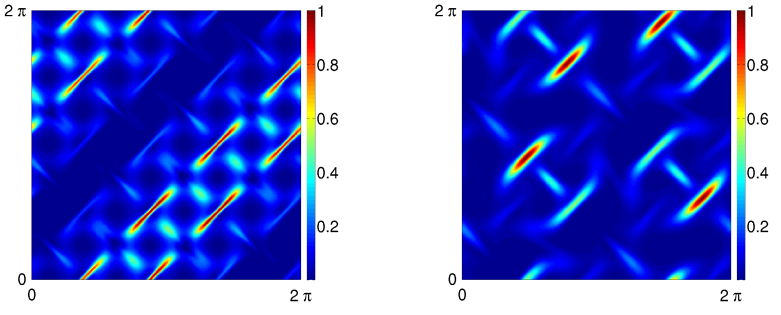

FIGURE 13. Contour of the magnetic energy B_{2D} for the two different laminar flows at two different Re - Left $Re_{T_1} < Re \approx 5.4 < Re_{T_2}$, Right $Re \approx 0.53 < Re_{T_1}$. The contours correspond to the nonhelical forcing case.

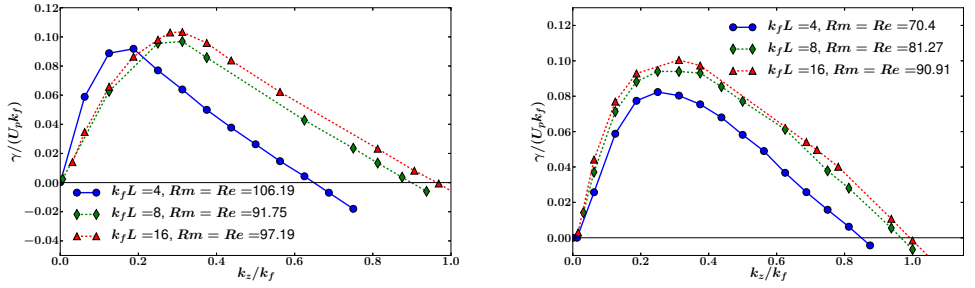

FIGURE 14. Figure shows $\gamma/(U_p k_f)$ as a function of k_z/k_f for different values of k_f for helical forcing shown on left and nonhelical forcing shown on the right. The kinetic Reynolds number and the magnetic Reynolds number are mentioned in the legends.

7. Dependence on $k_f L$

In this section we extend our study to flows with higher values of $k_f L$. The linear damping coefficient is adjusted for each value of $k_f L$ so that maximum inertial range for the inverse cascade is obtained without forming condensates. As we increase $k_f L$ the large scale inverse cascade becomes more important. Depending on the forcing used and the scale seperation the relative amplitude of u_{2D} and u_z change as we change $k_f L$. In order thus to have a fair comparison between the different dynamos we normalize the growth rates based on the results of the Ponomarenko dynamo (Ponomarenko 1973), where the growth rate is proportional to the product of the vertical velocity $\mathbf{u_z}$ and the planar velocity $\mathbf{u_{2D}}$ divided by the total rms value. Thus we define a velocity scale, $U_p = (\langle|\mathbf{u_{2D}}|^2\rangle^{1/2} \langle u_z^2\rangle^{1/2})/(\langle|\mathbf{u_{2D}}|\rangle^2 + \langle|u_z|\rangle^2)^{1/2}$ with which we normalize the growth rate. Figure 14 shows normalized growth rate $\gamma/(U_p k_f)$ as a function of normalized modes k_z/k_f for both the helical and nonhelical forcing as we increase $k_f L$ for similar values of Re, Rm. Since k_f is increased the growth rate γ and the number of unstable k_z modes increase. This behaviour is similar for both the helical and nonhelical forcing case. The normalized curves seems to follow similar trend for both the forcing cases considered here. At relative large Rm and as the scale separation is increased the most unstable wave number appears to be close to the forcing wavenumber $k_z^{max} \approx \frac{1}{3} k_f$ in both helical and nonhelical forcing cases. This implies that the most unstable modes have similar length scale with forcing and not with the box size.

The normalized maximum growth rate $\gamma_{max}/(U_p k_f)$ and the normalized cut-off wavenumber k_z^c/k_f for both helical and nonhelical forcing are shown in figure 15. As can be seen from the figures the normalized quantities follow similar trends to $k_f L = 4$ with weak (or no) dependence on the box size L. Hence the inverse cascade does not seem to affect the dynamo instability, as is expected since the mechanisms of small scale dynamo effect and the α-dynamo are mostly governed by the forcing scale or scales smaller than the forcing scale where the strongest shear exists.

8. Conclusions

The dynamo instability in the $2.5D$ configuration is studied for a wide range of control parameters. This allowed us to test certain limits that are still not attainable in three dimensional simulations.

For helical flows we were able to test the alpha dynamo predictions for the behaviour of the large scales ($k_z \ll k_f$) both for small and large values of Rm, Re. The analytical

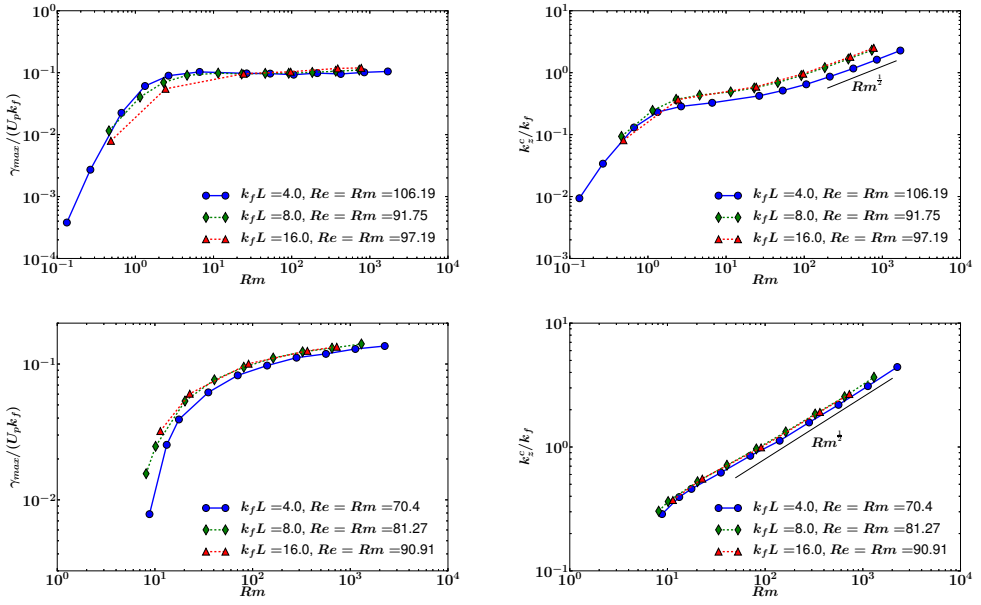
$\gamma_{max}/(U_p k_f)$
k_z^c/k_f
Rm
$Rm^{\frac{1}{2}}$
$k_f L$ =4.0, $Re = Rm$ =106.19
$k_f L$ =8.0, $Re = Rm$ =91.75
$k_f L$ =16.0, $Re = Rm$ =97.19
$k_f L$ =4.0, $Re = Rm$ =70.4
$k_f L$ =8.0, $Re = Rm$ =81.27
$k_f L$ =16.0, $Re = Rm$ =90.91

FIGURE 15. Plots of normalized growth rate - $\gamma_{\max}/(U_p k_f)$ on the left and k_z^c/k_f on the right for 1. Top - helical forcing and 2. Bottom - nonhelical forcing as a function of Rm for different $k_f\, L$ mentioned in the legends.

predictions of mean field theories for small values of Rm were verified. For large values of Rm the growth rates were also shown to be in agreement with a turbulent alpha dynamo (calculated numerically from equations 4.2, 4.3), and the isotropic α was shown to asymptote to a value independent of Re and Rm. Nonetheless, at large Rm the large scale modes were not the most unstable ones. At sufficiently large Rm the fastest growing mode was always found to have k_z close to the forcing wavenumber. Thus in a three dimensional simulation with random initial conditions for the magnetic field, it is the scales close to the forcing that would be observed in the linear stage of the dynamo. This of course does not imply that the large scale instability does not play a role in the saturated stage of the dynamo and the formation of large scale magnetic fields at high Rm. To resolve this issue however a nonlinear formalism for the alpha dynamo would be required.

The non-helical forcing was also shown to result in dynamo instability above a value of the magnetic Reynolds number with similar behaviour in the small scales $k_z \gtrsim k_f$ as the helical dynamo. The critical value of the magnetic Reynolds number for a thin layer of height H was shown to scale like $Rm_c^H \propto Re^{2\zeta}/\sqrt{H}$ with $\zeta \simeq 1/4$ for nonhelical flows and $\zeta \simeq 3/8$ for helical flows, implying that there is a dependence of Rm_c^H on Re even at large values of Re. At infinite layer thickness H the helical flow always resulted in to dynamo (ie $Rm_c = 0$). On the other hand the non-helical flow Rm_c was reaching asymptotically a finite value in the limit $Re \to \infty$.

The investigated dynamo flows were motivated by rotating flows that tend to become two dimensional at sufficiently large rotation rates. In nature rotating flows are never fully two-dimensionalized. Even in fast rotating flows large two-dimensional motions co-exist with three dimensional perturbations either in the form of turbulent eddies or travelling inertial waves. The resulting dynamo then is in general the result of a combination these effects. However, due to the fast decorrelation time of eddies and inertial waves that has

a suppressing effect for dynamo we expect that at fast rotating flows 2.5D flows could play the dominant effect for dynamo. Rotation could thus also provide a mechanism to improve the dynamo experiments. Such an expectation can be verified by a study of the full three dimensional dynamo flow subject to fast rotation.

The authors would like to thank F. Petrelis, S. Fauve and B. Gallet for their very useful comments and fruitful discussions. The present work benefited from the computational support of the HPC resources of GENCI-TGCC-CURIE & GENCI-CINES-JADE (Project No. x2014056421 & No. x2015056421) and MesoPSL financed by the Region Ile de France and the project EquipMeso (reference ANR-10-EQPX-29-01) where the present numerical simulations have been performed.

REFERENCES

Alexakis, A. 2015 Rotating taylor–green flow. *J. Fluid Mech.* **769**, 46–78.

Bartello, P., Metais, O. & Lesieur, M. 1994 Coherent structures in rotating three-dimensional turbulence. *J. Fluid Mech.* **273**, 1–29.

Batchelor, G. K. 1959 Small-scale variation of convected quantities like temperature in turbulent fluid part 1. general discussion and the case of small conductivity. *J. Fluid Mech.* **5** (01), 113–133.

Boffetta, G. 2007 Energy and enstrophy fluxes in the double cascade of two-dimensional turbulence. *J. Fluid Mech.* **589**, 253–260.

Campagne, A., Gallet, B., Moisy, F. & Cortet, P.-P. 2014 Direct and inverse energy cascades in a forced rotating turbulence experiment. *Phys. Fluids* **26** (12), 125112.

Chen, Q., Chen, S., Eyink, G. L. & Holm, D. D. 2005 Resonant interactions in rotating homogeneous three-dimensional turbulence. *J. Fluid Mech.* **542**, 139–164.

Childress, S. 1969 A class of solutions of the magnetohydrodynamic dynamo problem. *The Application of Modern Physics to the Earth and Planetary Interiors* pp. 629–648.

Courvoisier, A., Hughes, D. W. & Tobias, S. M. 2006 α effect in a family of chaotic flows. *Phys. Rev. Lett.* **96** (3), 034503.

Davidson, P. A. 2014 The dynamics and scaling laws of planetary dynamos driven by inertial waves. *Geophys. J. Int.* **198** (3), 1832–1847.

Deusebio, E., Boffetta, G., Lindborg, E. & Musacchio, S. 2014 Dimensional transition in rotating turbulence. *Phys. Rev. E* **90** (2), 023005.

Gallet, B. 2015 Exact two-dimensionalization of rapidly rotating large-reynolds-number flows. *J. Fluid Mech.* **783**, 412–447.

Gallet, B., Campagne, A., Cortet, P.-P. & Moisy, F. 2014 Scale-dependent cyclone-anticyclone asymmetry in a forced rotating turbulence experiment. *Phys. Fluids* **26** (3), 035108.

Galloway, D. J. & Proctor, M. R. E. 1992 Numerical calculations of fast dynamos in smooth velocity fields with realistic diffusion. *Nature* **356**, 691 – 693.

Gilbert, A. D. 2003 Dynamo theory. *Handbook of mathematical fluid dynamics* **2**, 355–441.

Gomez, D. O., Mininni, P. D. & Dmitruk, P. 2005 Parallel simulations in turbulent mhd. *Phys. Scr.* **T 116**, 123.

Hopfinger, E. J. & van Heijst, G. J. F. 1993 Vortices in rotating fluids. *Annu. Rev. Fluid Mech.* **25**, 241–289.

Hossain, M. 1994 Reduction in the dimensionality of turbulence due to a strong rotation. *Phys. Fluids* **6**, 1077–1080.

Iskakov, A. B., Schekochihin, A. A., Cowley, S. C., McWilliams, J. C. & Proctor, M. R. E. 2007 Numerical demonstration of fluctuation dynamo at low magnetic prandtl numbers. *Phys. Rev. Lett.* **98** (20), 208501.

Izakov, M. N. 2013 Large-scale quasi-two-dimensional turbulence and a inverse spectral flux of energy in the atmosphere of Venus. *Solar Syst. Res.* **47**, 170–181.

Lanotte, A., Noullez, A., Vergassola, M. & Wirth, A. 1999 Large-scale dynamo

produced by negative magnetic eddy diffusivities. *Geophys. Astrophys. Fluid Dyn.* **91** (1-2), 131–146.

Mininni, PD 2007 Inverse cascades and α effect at a low magnetic prandtl number. *Phys. Rev. E* **76** (2), 026316.

Mininni, P. D. & Pouquet, A. 2010 Rotating helical turbulence. I. Global evolution and spectral behavior. *Phys. Fluids* **22** (3), 035105.

Pedlosky, J. 1987 *Geophysical fluid dynamics*. New York, Springer.

Ponomarenko, Yu B 1973 On the theory of the hydrodynamic dynamo. *J. Appl. Mech. Tech. Phys* **14**, 775–779.

Ponty, Y., Mininni, P. D., Montgomery, D. C., Pinton, J-F., Politano, H. & Pouquet, A. 2005 Numerical study of dynamo action at low magnetic prandtl numbers. *Phys. Rev. Lett.* **94** (16), 164502.

Proctor, M. R. E. & Gilbert, A. D. 1995 *Lectures on Solar and Planetary Dynamos*.

Roberts, G. O. 1972 Dynamo action of fluid motions with two-dimensional periodicity. *Phil. Trans. R. Soc.* **271** (1216), 411–454.

Scott, J. F. 2014 Wave turbulence in a rotating channel. *J. Fluid Mech.* **741**, 316–349.

Sen, A., Mininni, P. D., Rosenberg, D. & Pouquet, A. 2012 Anisotropy and nonuniversality in scaling laws of the large-scale energy spectrum in rotating turbulence. *Phys. Rev. E* **86** (3), 036319.

Smith, L. M. & Waleffe, F. 1999 Transfer of energy to two-dimensional large scales in forced, rotating three-dimensional turbulence. *Phys. Fluids* **11**, 1608–1622.

Smith, S. G. L. & Tobias, S. M. 2004 Vortex dynamos. *J. Fluid Mech.* **498**, 1–21.

Staplehurst, P. J., Davidson, P. A. & Dalziel, S. B. 2008 Structure formation in homogeneous freely decaying rotating turbulence. *J. Fluid Mech.* **598**, 81–105.

Sugihara, Y., Migita, M. & Honji, H. 2005 Orderly flow structures in grid-generated turbulence with background rotation. *Fluid Dyn. Res.* **36**, 23–34.

Thiele, M. & Müller, W.-C. 2009 Structure and decay of rotating homogeneous turbulence. *J. Fluid Mech.* **637**, 425.

Tobias, S. M. & Cattaneo, F. 2008 Dynamo action in complex flows: the quick and the fast. *J. Fluid Mech.* **601**, 101–122.

van Bokhoven, L. J. A., Clercx, H. J. H., van Heijst, G. J. F. & Trieling, R. R. 2009 Experiments on rapidly rotating turbulent flows. *Phys. Fluids* **21** (9), 096601.

Waleffe, F. 1993 Inertial transfers in the helical decomposition. *Phys. Fluids* **5**, 677–685.

Yarom, E., Vardi, Y. & Sharon, E. 2013 Experimental quantification of inverse energy cascade in deep rotating turbulence. *Phys. Fluids* **25** (8), 085105.

Yeung, P. K. & Zhou, Y. 1998 Numerical study of rotating turbulence with external forcing. *Phys. Fluids* **10**, 2895–2909.

Yoshimatsu, K., Midorikawa, M. & Kaneda, Y. 2011 Columnar eddy formation in freely decaying homogeneous rotating turbulence. *J. Fluid Mech.* **677**, 154–178.

Zel'dovich, Ya. B. 1958 Electromagnetic interaction with parity violation. *Sov. Phys. JETP* **6**, 1184, [Zh. Eksp. Teor. Fiz. 33, 1531 (1957)].